Nuclear Materials and Energy 41 (2024) 101806

Contents lists available at ScienceDirect

Nuclear Materials and Energy

journal homepage: www.elsevier.com/locate/nme

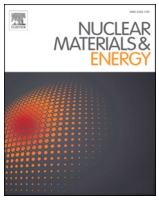

Investigation of H-mode density limit in mixed protium–deuterium plasmas at JET with ITER-like wall

A. Huber [a,*], G. Sergienko [a], M. Groth [b], D. Keeling [c], M. Wischmeier [d], D. Douai [e], E. Lerche [f], C. Perez von Thun [g], S. Brezinsek [a], V. Huber [h], A. Boboc [c], M. Brix [c], I.S. Carvalho [i], A.V. Chankin [d], E. Delabie [j], I. Jepu [c], V. Kachkanov [c], V. Kiptily [c], K. Kirov [c], Ch. Linsmeier [a], E. Litherland-Smith [c], C.G. Lowry [k,l], C.F. Maggi [c], J. Mailloux [c], A.G. Meigs [c], Ph. Mertens [a], M. Poradzinski [c,m], K.-D. Zastrow [c], M. Zlobinski [a], JET contributors[1], the EUROfusion Tokamak Exploitation team[2]

[a] Forschungszentrum Jülich GmbH, Institut für Energie- und Klimaforschung – Plasmaphysik, Partner of the Trilateral Euregio Cluster (TEC), 52425 Jülich, Germany
[b] Aalto University, Espoo, Finland
[c] CCFE, Culham Science Centre, Abingdon OX14 3DB, UK
[d] Max-Planck-Institut für Plasmaphysik, D-85748 Garching, Germany
[e] CEA, IRFM, Association Euratom-CEA, 13108 St. Paul lez Durance, France
[f] LPP-ERM/KMS, Association EUROFUSION-Belgian State, TEC partner, Brussels, Belgium
[g] Institute of Plasma Physics and Laser Microfusion (IPPLM), Warsaw, Poland
[h] Forschungszentrum Jülich GmbH, Supercomputing Centre, 52425 Jülich, Germany
[i] Instituto de Plasmas e Fusão Nuclear, Instituto Superior Técnico, Universidade de Lisboa, Portugal
[j] Oak Ridge National Laboratory, Oak Ridge, TN, USA
[k] JET Exploitation Unit, Culham Science Centre, Abingdon OX14 3DB, UK
[l] European Commission, B1049 Brussels, Belgium
[m] Institute of Plasma Physics and Laser Microfusion, Hery 23 Street, 01-497 Warsaw, Poland

ARTICLE INFO

Keywords:
Density limit
H-mode
Detachment
Greenwald fraction
JET
ILW

ABSTRACT

Analysis of comparable discharges fuelled by either deuterium or protium reveals a clear relationship between the isotope mass and the H-mode density limit. Notably, the density limit is significantly lower in protium, showing a reduction of up to 35 % compared to identical deuterium plasma conditions. Within mixed H-mode density limit (HDL) plasmas, the maximum achievable density, or H-mode density limit, decreases with increasing protium concentration, denoted as c_H. For instance, the highest corresponding maximum Greenwald fraction (f_{GW}) of about 1.02 was observed in the pulse with the lowest c_H value of 4.4 %. This f_{GW} decreases to 0.96 at $c_H = 48$ %. The average atomic mass, $\overline{A}$, of the plasma species decreases in these pulses from the value of 1.96 ($c_H = 4.4$ %) down to 1.52 ($c_H = 48$ %). Interestingly, the maximum achievable density appears to be largely unaffected by the applied power value, regardless of whether deuterium or protium is used, as well as under mixed H/D fuelling conditions.

Additionally, the measured Greenwald fractions are agreed with a heuristic model based on the SOL pressure threshold of an MHD instability, as proposed by Goldston. This comparison, especially concerning the model's dependence on isotopic mass, shows full consistency between the measured and predicted Greenwald fractions.

* Corresponding author at: Institut für Energieforschung-Plasmaphysik, Forschungszentrum Jülich GmbH, 52425 Jülich, Germany.
E-mail address: A.Huber@fz-juelich.de (A. Huber).

[1] See the author list of "Overview of T and D-T results in JET with ITER-like wall" by CF Maggi et al. to be published in Nuclear Fusion Special Issue: Overview and Summary Papers from the 29th Fusion Energy Conference (London, UK, 16-21 October 2023).

[2] See the author list of "Overview of the EUROfusion Tokamak Exploitation programme in support of ITER and DEMO" by E. Joffrin Nuclear Fusion 2024 10.1088/1741-4326/ad2be4.

https://doi.org/10.1016/j.nme.2024.101806
Received 13 June 2024; Received in revised form 21 October 2024; Accepted 4 November 2024
Available online 6 November 2024

1. Introduction

The baseline operational scenario envisioned for ITER [1], DEMO [2], and future fusion power plants involves operating in high confinement mode (H-mode) with a partially or fully detached divertor at the highest possible densities. Achieving a detached divertor at high densities is crucial for maximizing fusion power and successfully operating future reactors with reduced thermal heat loads on the plasma-facing components.

However, at sufficiently high densities, a back-transition from H-mode to low confinement mode (L-mode) is observed. The density is constrained by the so-called Greenwald limit, an operational threshold for density in magnetic confinement devices [3]:

$$n_{GW} = \frac{I_p}{\pi a^2} \tag{1}$$

where n_{GW} is the *line averaged* density in 10^{20} m^{-3}, I_p the plasma current in MA, and a the minor radius in m.

The H-mode density limit (HDL) in D-plasmas typically occurs at Greenwald fractions ($f_{GW} = \overline{n_e}/n_{GW}$) of 0.8–1.1 [3] and is assumed by R. Goldston [4] to be caused by the MHD instability in the SOL near the separatrix. However, it should be noted that there is no common acceptance of the physics behind the H-L transition. The publication [5] concluded that the HDL is not linked to reaching the ballooning mode limit.

Density limit studies have been intensively conducted in the last ten years on machines with fully metallic walls such as JET and AUG machines [6,7]. Despite considerable efforts, not all the underlying mechanisms responsible for the H-L transition are comprehensively understood. Specifically, the influence of isotope effects can significantly affect the HDL. Most H-mode density studies have been performed in pure D plasma, with only a few experiments in pure H [8] and He plasmas [8]. At JET-ILW, by comparing similar discharges fueled with either deuterium or protium, it was shown that the H-mode density limit in protium is 35 % lower compared to similar deuterium plasma conditions, as depicted in Fig. 1.

Both plasma discharges have been carried out in a similar vertical target magnetic field configuration with $I_p/B_T = 1.9$ MA/1.8 T and $q_{95} = 2.8$. The observed HDL pulses in JET, in both protium and deuterium plasmas, exhibit similar operational phases, indicating identical physical processes underlying the H-L transition.

Despite successful research in pure plasmas with different hydrogen isotopic species, the HDL in mixed plasmas remains unexplored. Given that both ITER, DEMO, and future fusion devices will operate with mixed deuterium/tritium plasmas, understanding the physics of the H-L transition in mixed plasmas is crucial. However, experiments on HDL in mixed D/T plasmas are complex and consume a significant portion of the tritium budget allocated for allowable tritium injection during DT campaigns. Therefore, a mixture of H and D in JET-ILW is selected for the HDL study during the D campaign.

In this contribution, for the first time, the influence of the hydrogen isotope mixture on the HDL in the fully metallic machine JET-ILW is investigated. Additionally, the measured Greenwald fractions are compared to a heuristic model based on the SOL pressure threshold of an MHD instability as proposed by Goldston [4], particularly regarding the theory's dependence on isotopic mass. The magnetic field configuration in the analyzed pulse was as depicted in Fig. 5b and Fig. 6b and remained consistent across all analyzed pulses.

2. Experimental results

2.1. H-mode density limit experiment in mixed protium–deuterium plasmas at JET with ITER-like wall

To explore the impact of different compositions of mixed protium-deuterium plasmas on the HDL, a series of experiments commenced on JET with ITER-like wall (JET-ILW): beryllium in the main chamber and tungsten in the divertor. The standard scenario for these investigations involves a gas ramp discharge with a plasma current of $I_p = 1.85$ MA, a toroidal magnetic field on-axis of $B_T = 1.85$ T, corresponding to a q_{95} of approximately 3.2. The average configuration triangularity falls within the low range, approximately $\delta_{av} \approx 0.26$. Auxiliary heating power of around $P_{heat} = 8.0$–10.0 MW is applied to the discharges, exceeding the L-H power threshold of about $5.0 - 6.5$ MW. The ohmic heating power in the investigated plasma pulses is about 1 MW. The $P_{L\text{-}H}$ threshold is defined by the ITPA scaling law [9], established by Y. Martin, taking into account the dependence of the threshold power on the ion mass number (M_{eff}): $P_{L\text{-}H} \propto 1/M_{eff}$.

This HDL represents an effective, non-disruptive density constraint, known as a 'soft limit', as it entails a back transition to L-mode, allowing plasma operation to continue with lower confinement. Please note that this is not a universal phenomenon observed across all tokamak devices. For instance, in JET-ILW, the central averaged density decreases following the H-L transition, and L-mode remains sustainable. However, in ASDEX Upgrade tokamak, the plasma density increases during the unsustainable L-mode, eventually reaching the L-mode density limit, which ultimately results in a disruption [5,7].

In order to minimize total gas consumption, experiments with mixed hydrogen isotopes were performed using a "warm" cryopump with

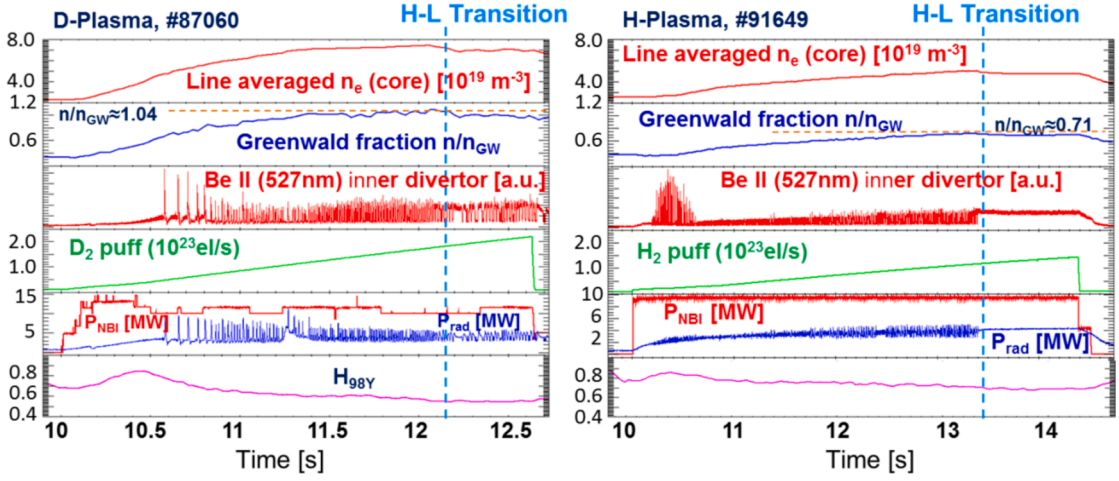

Fig. 1. Time traces from a standard density ramp-up experiment conducted on JET-ILW with D-plasma (left) and H-plasma (right). The onset of the HDL limit is indicated by dashed lines.

divertor cryo-panels cooled with liquid nitrogen (LN2). It is worth noting that conducting of high-density experiments with cryo at LN2 temperature on the JET-C with a carbon divertor was previously unfeasible due to substantial fuel retention in the wall and significant gas outgassing during plasma pulses, leading to inadequate plasma density control. However, this has changed with the entire JET wall being equipped with metallic plasma-facing components (PFC), reducing fuel retention by a factor of 10 and significantly decreasing wall outgassing during plasma pulses [10]. By operating the JET-ILW vessel with reduced divertor pumping speed, we replicate conditions similar to the base gas pressure on ITER, ensuring the experiments are directly relevant. We conducted the experiment with a base pressure of 1.55×10^{-6} mbar before initiating the HDL pulses with a warm cryopump. This is significantly higher than the typical base pressure at JET-ILW with a cold cryopump, which usually ranges from 10^{-7} to 10^{-8} mbar. ITER aims for a base pressure of 5×10^{-6} mbar before each pulse [11], and the pressure achieved in our experiments closely matches these conditions, making the results applicable to ITER's operational environment.

Fig. 2 illustrates the comparison between HDL pulses in JET-ILW with cold and warm cryo-pumps. The graph depicts the line-averaged density versus gas injection rate for these pulses. Remarkably, the HDL remains consistent between the cold and warm cryo-pump experiments, despite the differences in neutral pressure in the SOL. A detailed discussion of the impact of detachment on the HDL is beyond the scope of this paper. Detachment physics, however, strongly depends on the neutral pressure in the SOL and may vary between cold and warm cryopump conditions. However, we should reference an earlier assertion that detachment plays a negligible role in the H-L transition in fully metallic wall machines [7,28]. Furthermore, all phases typically observed in HDL pulses with cold cryo-pumps are also evident in pulses with warm cryo-pumps. Notably, the total gas consumption is reduced by a factor of 13 in plasmas utilizing warm cryopumps. In the following, we will discuss the H-mode density experiments performed under the warm cryo-pump condition.

2.2. Time evolution of a typical HDL gas ramp discharge

Fig. 3 displays time traces of a typical H/D mixed HDL-plasma discharge in JET-ILW with a warm cryo-pump, with plasma parameters and shape as mentioned in section 2.1. To increase plasma density up to HDL, a gas ramp-up is implemented by external gas fuelling of neutral protium and deuterium. At the H-L transition, fuelling rates for H_2 and D_2 reach the values of 6.3×10^{21}H/s and 5.5×10^{21}D/s respectively. The D_2 was to a large extent fuelled into the inner and outer

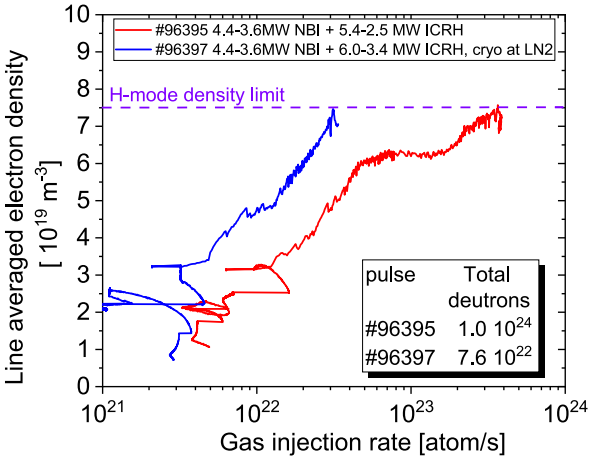

Fig. 2. Line averaged density versus gas injection rate for the plasma pulses with cold cryo-pump (#96395) and warm cryo-pump (#96397). The density evolution is shown only up to the starting of the density drop after the H-L transition.

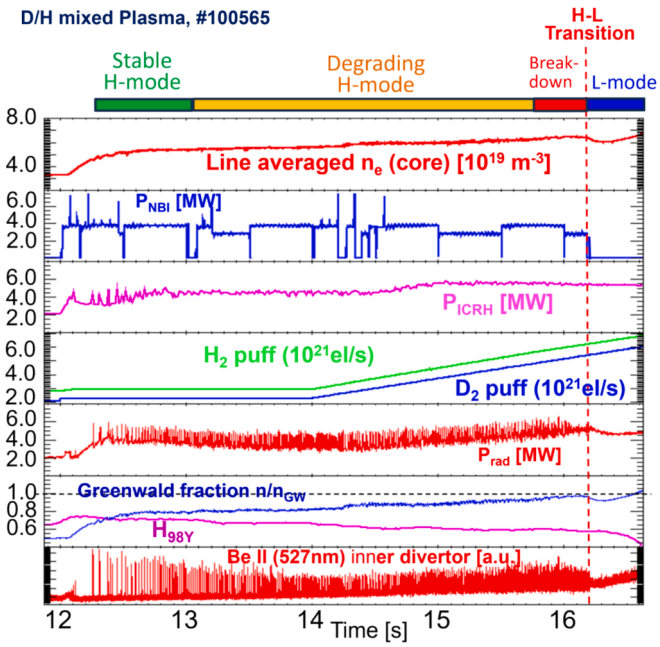

Fig. 3. Time evolution of a typical HDL discharge on JET-ILW.

divertor legs, H_2 mainly into the inner divertor. Additionally, a small amount of neutral particles was fuelled into the main chamber: H_2 at a constant rate of 2×10^{20} H/s and D_2 at another constant rate of 1.15×10^{21}D/s. During the gas ramp-up, the H concentration $c_H = n_H/(n_D + n_H)$ increases slightly (from 0.35 to 0.37), with a mean value of 0.37 at the H-L transition. The maximum achievable density is 6.4×10^{19}m^{-3} with a Greenwald fraction of about $f_{GW} = 0.98$. The total heating power ($P_{heat} = P_{NBI} + P_{ICRH} + P_{ohmic}$) of 9.5 MW, along with the bulk radiation power $P_{rad}^{bulk} = 1.5-1.7MW$, ensures that the discharge at the H-L transition time is above the 6.5 MW L-H power threshold, as defined by the ITPA scaling law [9], established by Y. Martin, taking into account the ion mass dependence of fuel species. Immediately after the H-L transition, following a very short period, the tripping of the NBI beams (the shutdown of all NBI beams) was often observed at JET-ILW. This tripping is triggered by the H-L transition, which leads to an abrupt increase in the neutral pressure inside the NBI duct. There is a certain threshold of neutral pressure beyond which the protection system stops the operation of the NBI beams. This protective action is intended to avoid the reionization of the NBI neutral atoms, which could be deflected in the NBI duct toward the wall and potentially cause serious damage to the duct wall. NBI operates in interlaced mode, delivering 4 MW on average. Fig. 3 also shows the *Be II* fast emission signal in the divertor, indicating ELM behavior during density ramp-up. The confinement remains constant ($H_{98Y} = 0.71$) up to $n_e/n_{GW} = 0.8$. Supplementary gas puffing leads to a moderate increase of the density, but the confinement deteriorates strongly down to $H_{98Y} = 0.57$, usually transitioning to L mode.

This H/D mixed HDL pulse exhibits similar operational phases (stable H-mode, degrading H-mode, breakdown of H-mode, and L-mode) as observed in pure H and D plasmas [6,7]. These phases are indicated with colored bars at the top of Fig. 3. Similar to the HDL experiments in pure H and D plasmas, a sequence of H-L-H transitions, known as the 'dithering H-mode' phase, has been observed prior to the final transition into L-mode during both the "Degrading H-mode" and the "Breakdown of H-mode" phases. The intensive discussion about the 'dithering H-mode' can be found in [6,8], and it is beyond the scope of this paper.

The total radiated power, measured with help of the metallic resistance bolometer system [12], increases slightly during the H-mode phase up to the H-L transition, from 4.0 MW to 4.9 MW. The observation that the radiation fraction remains around $\gamma_{rad} = P_{rad}/P_{heat} = 0.52$

without any significant change during the density ramp-up indicates that the HDL is neither associated with additional energy losses from the confined region due to radiation nor with an inward collapse of the hot discharge core caused by overcooling of the plasma periphery from radiation. The effective ion charge, Z_{eff}, ranges around 1.6 during the density ramp-up pulses.

2.3. Impact of the H/D composition on the H-mode density limit

Plasma pulses under identical plasma conditions but with different c_H was carried out in mixed H/D plasmas. The plasmas were heated using deuterium neutral beam injection and ICRH, and the heating power, magnetic configuration, and H_2/D_2 gas fuelling locations remained consistent throughout the experiments. Fig. 4 shows the time traces of line-averaged densities in the HDL pulses with varying concentrations of protium, c_H. Measurements of *D* and *H* concentrations in the JET sub-divertor region were conducted using Optical Penning Gauge Spectroscopy [13,14]. The sub-divertor region specifically refers to the part of the divertor located below (or underneath) the primary divertor target plates.

The maximum achievable density, i.e., the HDL decreases with increasing c_H concentration. The corresponding maximum Greenwald fraction was approximately 1.02 in the pulse with the smallest $c_H = 4.4$ %. This fraction f_{GW} decreases to 0.96 at $c_H = 48$ %. The average atomic mass, $\overline{A}$, of the plasma species reduces in these pulses from value of 1.96 ($c_H = 4.4$ %) to 1.52 ($c_H = 48$ %).

The Goldston model ($f_{GW,Goldston} \propto \overline{A}^{9/16}$) predicts a slightly larger reduction than observed in this experiment; for instance, at $c_H = 48$ %, the predicted f_{GW} is 0.89, whereas the experiment shows $f_{GW} = 0.96$. This disparity could be explained by the Goldston model suggesting that the HDL is caused by MHD instability in the SOL near the separatrix and that the isotopic composition at the separatrix and in the sub-divertor region is not identical. Further discussion on this topic is provided in the following sections.

2.4. Isotope ratio composition in the scrape-off layer (SOL)

At JET-ILW, the isotope ratio in the scrape-off layer (SOL) in the main chamber as well as in the divertor is measured using passive H_α high-resolution spectroscopy (HRS):

The high-resolution divertor spectroscopy system on JET, referred in this paper as the KSRB diagnostic, enables measurements of Balmer-alpha deuterium and protium spectral lines with a resolving power of $\lambda/\Delta\lambda \approx 27000$ and a Full Width at Half Maximum (FWHM) of the instrumental function of $\Delta\lambda_{ins} = 0.024$ nm. With 10 lines-of-sight (LOS)

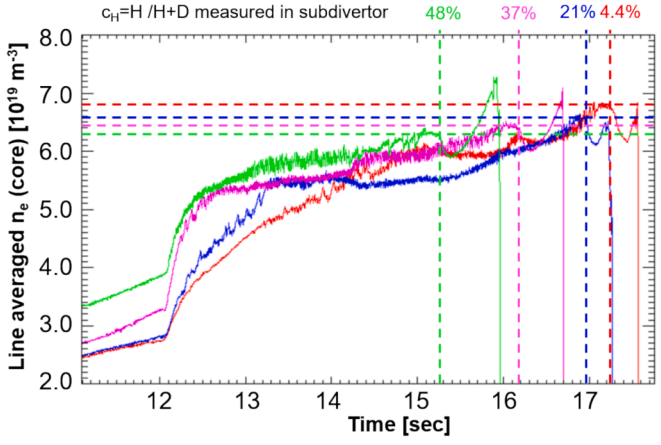

Fig. 4. The time traces of the line-averaged densities in the H-mode density limit pulses with different concentrations of protium, c_H.

observed from the top of the machine, the KSRB spectrometer covers the outer divertor. Fig. 5b displays the poloidal cross-section of the JET-ILW divertor with the lines of sight (LOS) of the KSRB spectroscopy system.

High-resolution main chamber H_α spectroscopy is based on an Echelle overview spectrometer (Spectrelle 20000p, Systematix and GWU Lasertechnik GmbH cooperation, 110 mm focal length) with radial LOS provides the high resolution measurements in the wavelength range of 365–720 nm. The resolving power of the spectrometer is approximately $\lambda/\Delta\lambda \approx 20000$ and the FWHM of the instrument function is about $\Delta\lambda_{ins} = 0.033$ nm. The radial LOS is directed towards the inner wall in the main chamber (recessed W-coated CFC tile) (see Fig. 6b). It is important to note that measurements in the main chamber SOL present challenges in signal decomposition, particularly in separating the light from the SOL on the high field side (HFS) and the SOL on the low field side (LFS). In this article, we focus on the mean value of the isotope ratio averaged over the HFS and LFS SOLs.

Fig. 5 shows spectra observed in the mixed H/D plasmas shortly before the H-L transitions. The spectral lines represent line-integrated contributions along the line of sight indicated in Fig. 5b, which is directed towards the outer strike point in the divertor. To determine the *H/D* composition, a function comprising a sum of Gaussian distribution functions was fitted to the measured spectrum:

$$
\begin{aligned}
I_{fit}(\lambda) = a_0 + 2\sqrt{\frac{\ln 2}{\pi}}\Bigg[& I_{H_\alpha}\left(\frac{C_{Hc}}{\Delta\lambda_{coldH}}\exp\left(-\frac{\ln 2}{2}\left(\frac{\lambda-\lambda_{H_\alpha}}{\Delta\lambda_{Hcold}}\right)^2\right)\right. \\
& \left. + \frac{(1-C_{Hc})}{\Delta\lambda_{Hwarm}}\exp\left(-\frac{\ln 2}{2}\left(\frac{\lambda-\lambda_{H_\alpha}}{\Delta\lambda_{Hwarm}}\right)^2\right)\right) \\
& + I_{D_\alpha}\left(\frac{C_{Dc}}{\Delta\lambda_{Dcold}}\exp\left(-\frac{\ln 2}{2}\left(\frac{\lambda-\lambda_{D_\alpha}}{\Delta\lambda_{Dcold}}\right)^2\right)\right. \\
& \left. + \frac{(1-C_{Dc})}{\Delta\lambda_{Dwarm}}\exp\left(-\frac{\ln 2}{2}\left(\frac{\lambda-\lambda_{D_\alpha}}{\Delta\lambda_{Dwarm}}\right)^2\right)\right)\Bigg],
\end{aligned}
\tag{2}
$$

Where $\lambda_{H\alpha} = 656.279nm$ and $\lambda_{D\alpha} = 656.103nm$ [15] are the wavelengths for the H_α and D_α spectral lines of *H* and *D* atoms respectively, I_{H_α} and I_{D_α} are the total line intensities, $\Delta\lambda_{Hcold}$, $\Delta\lambda_{Dcold}$, $\Delta\lambda_{Hwarm}$ and $\Delta\lambda_{Hwarm}$ are full Width at Half Maximum (FWHM) for cold and warm components respectively, a_0, C_{Hc} and C_{Dc} are the fitting parameters. Similar to [16], we assume multiple fractions of atoms with different temperatures to characterize the spatial profile of the emissive layer along the LOS.

In this work, we utilize only two fractions, cold and warm, to characterize the spectral profile of each hydrogen species. With this approach, the fitting function aligns closely with the experimental spectral profile, as depicted in Fig. 5.

The $I_{fit}(\lambda)$ spectrum allows for the determination of the isotope concentration either using the cold fraction of atoms alone or by considering both fractions. In this work, we employ the approach of utilizing both fractions:

$$
c_H = \frac{n_H}{n_H + n_D} = \frac{I_{H_\alpha}}{I_{H_\alpha} + I_{D_\alpha}};\ c_D = \frac{n_D}{n_H + n_D} = \frac{I_{D_\alpha}}{I_{H_\alpha} + I_{D_\alpha}} \tag{3}
$$

In Fig. 5c, the determined c_H concentration is depicted as a function of c_H in the sub-divertor. Spectroscopically determined c_H concentration appears to be smaller than that measured in the sub-divertor (KT5P), with values ranging between 75 % and 100 % of the KT5P measurements. This variance can be attributed to the fact that divertor spectroscopy evaluates concentrations from line-integrated measurements along the line of sight of the emission layer, where the electron temperature T_e varies between 6 eV and approximately 30–40 eV.

Fig. 6 illustrates the results of fitting the measured spectral profile obtained with the Echelle survey spectrometer. The arrangement of the radial line of sight of the Echelle spectrometer to the JET inner wall area (W-coated CFC tiles) at octant 7 is depicted in Fig. 6b. The fitting function of Eq.2 comprising a sum of cold and warm components of both hydrogen species aligns well with the measured spectra. The evaluated

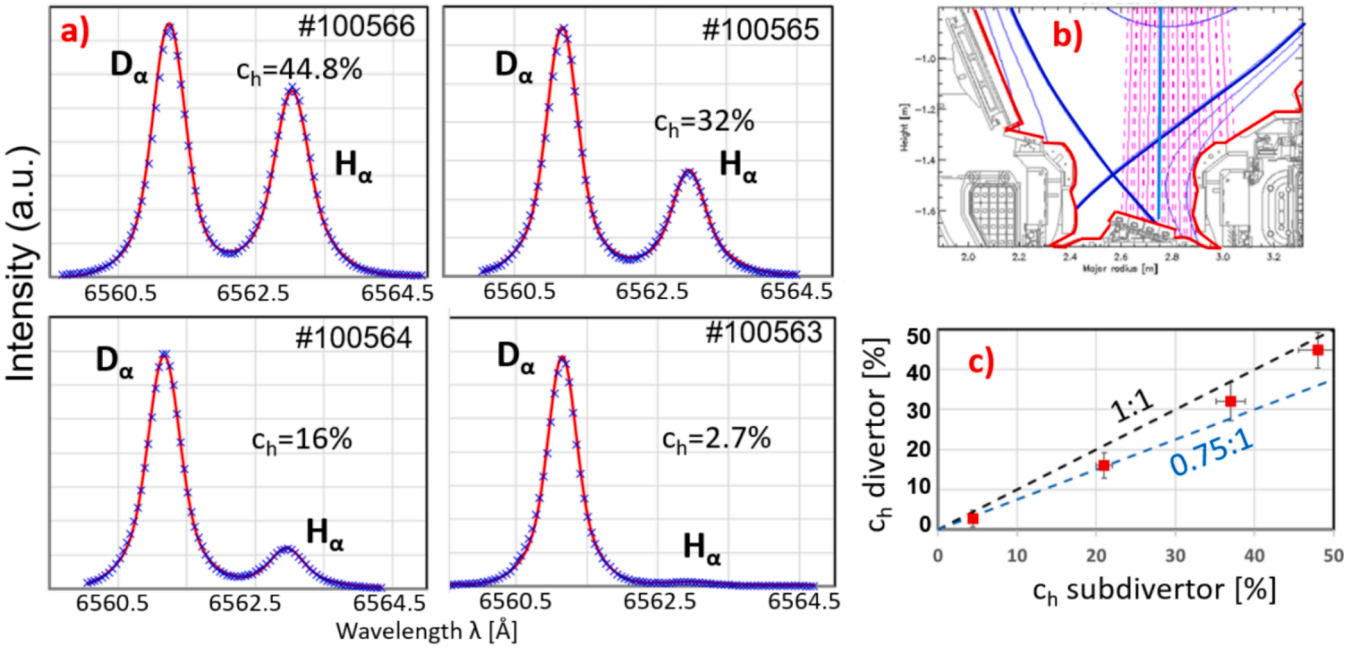

Fig. 5. A) Typical D_α/H_α spectra measured with high-resolution divertor spectrometers before the H-L transition in the mixed *H/D* plasmas with different *H/D* composition. The best fit to the measured spectra is shown by the solid line. b) Poloidal cross-sections of the JET-ILW divertor with lines of sight (LOS) of the KSRB divertor spectroscopy system c) Spectroscopically determined c_H concentration versus the c_H concentration measured in the sub-divertor (KT5P).

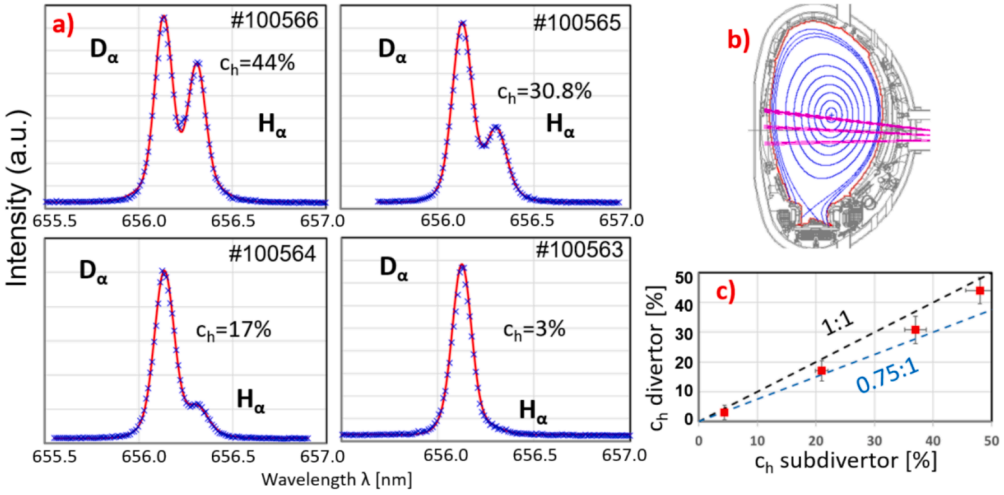

Fig. 6. A) typical d_α/H_α spectra measured with high-resolution main chamber H_α spectroscopy before the H-L transition in the mixed H/D plasmas with different H/D composition. The solid line represents the best fit to the measured spectra. b) Poloidal cross-sections of the JET-ILW divertor with lines of sight (LOS) of the Echelle overview spectrometer c) Spectroscopically determined c_H concentration versus the c_H concentration measured in the sub-divertor (KT5P).

c_H concentration exhibits a slight disparity (less than 25 % – the c_H values measured by Echelle specrometer consistently fall below the sub-divertor values) from the concentration measured in the sub-divertor.

The FWHM of the fitted Gaussian profiles can be expressed by $\Delta\lambda_{i,j}$:

$$\Delta\lambda_{ij} = 2\sqrt{\ln(2)}\lambda_{i\alpha}\sqrt{\frac{2kT_{ij}}{M_i c^2}} = 7.7\times10^{-5}\lambda_{i\alpha}\sqrt{\frac{T_{ij}}{M_i}} \quad (4)$$

where i is the hydrogen isotope index (H or D), j is component index (cold or warm), c is the speed of light, k is the Boltzmann constant, M_i is the mass of the hydrogen atoms in atomic units ($M_H = 1$ for H and $M_D = 2$ for D) and T_{ij} is the temperature of the hydrogen species in electron-volts.

In experiments with mixed H/D plasma, we observe that both the $\Delta\lambda_{icold}$ and $\Delta\lambda_{iwarm}$ values are nearly identical for H and D atoms, resulting in the best fit between $I_{fit}(\lambda)$ and the experimental data. Consequently, both hydrogen species, H and D, exhibit the same velocities but different energies. This finding aligns with a previous observation by A.N. Dmitriev [17], where almost identical velocities of H and D were reported in the SOL of tokamaks.

$T_{D,cold}$ varied in the studied plasma pulses from 3.9 eV to 6.2 eV for D atoms and $T_{H,cold}$ from 2.0 eV to 3.1 eV for H. These atoms, referred to as Franck-Condon atoms, result from the dissociation of molecules into the ground state and acquire Franck-Condon energies in the range of 2.2 eV. Upon interacting with the plasma in the SOL, these atoms could be heated to energies above 2.2 eV, as observed in the experiment. This process is described in detail in the following articles [18,19,20].

$T_{D,warm}$ of the hot fraction of deuterium atoms ranges from 36 eV to 42 eV, while $T_{H,warm}$ of the H atoms ranges from 18 eV to 21 eV. The

warm fraction of the hydrogen isotopes may arise from collisions between cold H/D atoms and fast H/D ions (charge exchange reaction). Additionally, the warm fraction may originate from D/H ions reflected on the W wall. At low energies, the reflection coefficient of the hydrogen isotope ions on W could be significant, exceeding 50 % [21].

In conclusion, the Balmer alpha spectral profile originates from the emission of recycled H/D on the wall, and the spectra reflect the hydrogen composition of the far SOL region.

3. Comparison with the theoretical model

The experimental results regarding the HDL limit from various tokamaks highlight the significant role of the edge plasma region, which extends from the separatrix into the scrape-off layer (SOL). In the current study by Eich et al. [22], it is demonstrated that the MHD normalized pressure gradient at the separatrix, denoted as $\alpha_{MHD,sep}$ in both fully-metal machines, AUG Upgrade and JET, exhibits a linear increase with n_{sep}/n_{GW}, where n_{sep} represents the density at the separatrix and n_{GW} is the Greenwald limit density. This analysis, as presented in [22] utilizes a comprehensive dataset encompassing a wide range of plasma parameters and confirms previous predictions by Goldston based on the heuristic drift-based model.

This model, proposed by R. J. Goldston [4], suggests that the HDL is caused by an MHD instability in the SOL close to the separatrix rather than originating in the core plasma or pedestal. As demonstrated in the study by Eich et al., $\alpha_{MHD,sep}$ reaches values around $\approx 2.0 - 2.5$, which were compared with the theoretically predicted onset of ballooning modes. For comparison, numerical calculations of global stability by Bernard et al. [23] yielded $\alpha_{crit} \approx \kappa^{1.2}(1+1.5\delta)$.

For typical triangularities in the analysed data base of $\delta = 0.2$ and elongations of $\kappa = 1.7$ one obtains $\alpha_{crit} \approx 2.5$. Numerical calculations by Makowski for DIII-D tokamak, just inside the separatrix, also give $\alpha_{crit} \approx 2.5$[24]. These values are in close consistency with the measured values by Eich et al., around $\approx 2.0 - 2.5$. In the subsequent analysis, we will utilize the expression $\alpha_{crit} \approx \kappa^{1.2}(1+1.5\delta)$ for the evaluating f_{GW}. Note that the critical ballooning parameter increases with increasing triangularity, resulting in larger HDL. This increase in the HDL with larger δ was experimentally observed in JET-ILW device [25].

Here in this paper, we will compare the HDL results with the Goldston model, which provides

$$f_{GW,Goldston} = 8.13\ C_\alpha \frac{\bar{n}}{n_{sep}} \left(\frac{q_{cyl}\ R\ B}{a} P_{SOL}\right)^{-1/8} (1+\kappa^2)^{\gamma-3/2} \left[\frac{2\bar{A}}{(1+\bar{Z})}\right]^{9/16} \left(\frac{Z_{eff}+4}{5}\right)^{-1/8} \quad (5)$$

where q_{cyl} is the cylindrical approximation for the safety factor, κ is the plasma elongation, R and a – the major and horizontal minor radiuses, $P_{SOL} = P_\Omega + P_{aux} - \frac{dW_{dia}}{dt} - P_{rad}^{bulk}$ is the power flowing from the core region into the SOL, P_Ω *and* P_{aux} are ohmic and auxiliary heating powers, P_{rad}^{bulk} is the radiated power from the bulk plasma, B is the total magnetic field strength, $\bar{n}$ *and* n_{sep} are the line-averaged and separatrix densities, Z_{eff} and $\bar{Z}$ are the "effective charge" and "average charge" of all ions.

The Goldston model assumes that the SOL β limit is defined by criticality to MHD instability and is characterized as $\alpha_{crit} = C_\alpha(1+\kappa^2)^\gamma$ with some parameters γ and C_α. By replacing this critical ballooning parameter through $\alpha_{crit} \approx \kappa^{1.2}(1+1.5\delta)$, the modified $f_{GW,Goldston}$ can be rewritten as:

$$f_{GW,Goldston} = 8.13\ \kappa^{1.2}(1+1.5\delta) \frac{\bar{n}}{n_{sep}} \left(\frac{q_{cyl}\ R\ B}{a} P_{SOL}\right)^{-1/8} (1+\kappa^2\ )^{-3/2} \left[\frac{2\ \bar{A}}{(1+\bar{Z})}\right]^{9/16} \left(\frac{Z_{eff}+4}{5}\right)^{-1/8} \quad (6)$$

The derived scaling shows small variations in the most important plasma parameters. At the same time, it shows a relatively strong dependence on the average atomic mass of the plasma ion species $\bar{A}$: $f_{GW} \propto \bar{A}^{\ 9/16}$. Note that the Greenwald fractions, f_{GW}, observed in JET-ILW experiments in H and D plasmas with wide range of variation of the plasma parameters are consistent with the Goldston's prediction [6,8]. In our comparative analysis, we used Greenwald fractions for the H/D mixed HDL plasmas, normalized to the f_{GW} in pure H-mode deuterium HDL plasma. The measured effective charge Z_{eff} was 1.6 and the estimated average ion charge $\bar{Z} \approx 1.12$ assuming *Be* as main impurity. All magnetic shape parameters (δ for triangularity and κ for elongation) in the investigated plasmas were identical. The electron density at the plasma edge in all the pulses, measured by High Resolution Thomson Scattering (HRTS) system [26], showed identical absolute values and profiles, corresponding to the same n_{sep}. The reference pulse with pure deuterium plasma shows f_{GW}, which agrees well with Goldston's prediction, up to a factor of 0.86: $f_{GW} \approx 0.86 \times f_{GW,Goldston}$. We assume that this factor is machine-independent and will be used for f_{GW} calculations.

As already mentioned, the model shows the strong dependence on the average atomic mass at the separatrix. As shown by M.Z. Tokar' [27], the plasma isotope composition in a tokamak reactor divertor scrape-off layer (SOL) changes along the magnetic field and can differ significantly from the gas composition in a pumping chamber. Thermal forces push heavier deuterons towards the higher temperature region, i.e. away from the divertor targets, and lighter hydrogen ions towards the colder divertor area. Hence, thermal forces can induce significant isotopic separation within the scrape-off layer (SOL), causing deuterium to accumulate far from the divertor plates at the equatorial plane. Additionally, the H/D composition in the far SOL may differ from that at the separatrix (c_D concentration at the separatrix larger than the c_D in the far SOL). Local measurement of the hydrogen composition at the separatrix is not feasible in any tokamak. However, spectroscopic measurement of the c_D/c_H ratio in the far SOL region at the midplane of JET provides the minimum boundary for the c_D value.

The H/D composition distribution also strongly depends on the plasma temperature T_0 ($T_e = T_i$ is assumed in the Tokar' analytical approch) in the main part of the SOL, which has maximum values at the

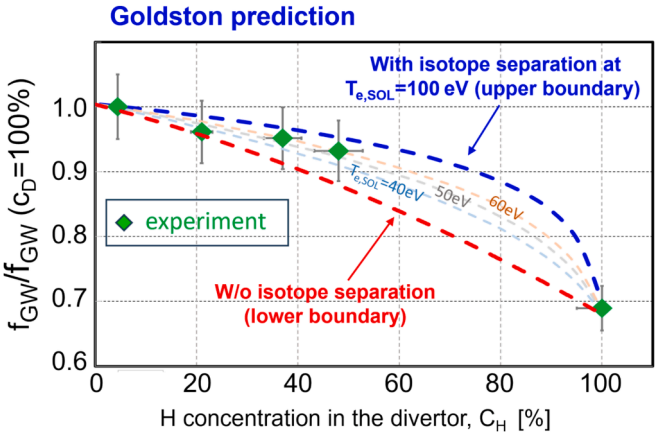

Fig. 7. Comparison between the measured values of the Greenwald fractions and the values predicted by the Goldston model.

separatrix in the vinicity of the stagnation point. This temperature correspond to the upstream separatrix temperature and can be calculated using the two-point model [29] of SOL transport and is about 100 eV.

Thus, Tokar's equations of the isotope separation in the SOL (taking into the account the maximum $T_0 = 100$ eV) establishes the upper boundary for the c_D value. Consequently, we can anticipate the operational parameter space where the HDL values of mixed plasmas are expected. Fig. 7 illustrates the operational parameter space in terms of Greenwald fractions and protium concentrations, c_H, measured in the subdivertor. The lower boundary curve represents the modified Goldston prediction of the Greenwald fraction, considering the c_H and c_D values measured by divertor spectroscopy, and therefore does not take into account isotope separation in the SOL. The upper boundary depicts the Goldston prediction using the c_H and c_D concentrations at the stagnation point predicted by Tokar's equations with $T_0 = 100$ eV. In this modelling, the segregation factor of protium $f_c = c_H$ *(divertor)* $/ c_H$ *(stagnation point)* is approximately 2.5, indicating significant isotopic separation of hydrogen within the SOL. In addition, the experimentally determined Greenwald fractions have been incorporated into the Fig. 7. Here, the f_{GW} values are normalized to the Greenwald fraction achieved in pure D plasma ($f_{GW}(c_D = 1.0)$). As depicted in Fig. 7, the experimental HDL values align well within the expected operational parameter space, thereby confirming Goldston's prediction.

Additionally, Fig. 7 represents the modified Goldston prediction, taking into account the isotope separation for different T_0 values: 40 eV, 50 eV, and 60 eV. One can see that the experimental values match well with the prediction for $T_0 \approx 50$ eV. This temperature is lower than $T_0 = 100$ eV, which is not surprising because the H-L transition process is initiated by ballooning instability in the outboard plasma region, where the temperatures are somewhat lower than those at the stagnation point.

4. Extrapolation to ITER

In this section we will try to predict the density limit for the ITER fusion device.

The design parameters for ITER in the baseline scenario (15MA Q = 10 inductive H-mode burning plasma discharges) are as follows [1]: $R = 6.2$ m, $a = 2.0$ m, $\kappa = 1.85$, $\delta = 0.48$, $B_T = 5.3$ T, $I_p = 15$MA, $q_{cyl} = 2.42$, $Z_{eff} = 1.6$, and $\overline{n}/n_{sep} = 3$. The ion ratio of the fusion fuel, $n_T/(n_D + n_T)$, is a key plasma parameter that must be tuned to maximize the power output of a tokamak fusion device and will be likely to be continuously monitored, for example, using neutron time-of-flight spectrometry. Assuming that ITER operates in deuterium–tritium (D-T) mixtures with 50 % D and 50 % T in the plasma core, the nominal operation of ITER with $Q = 10$ corresponds to $P_{SOL} = 100$ MW.

For such P_{SOL}, the expected separatrix electron temperature T_e, calculated from two-point model [29], at the stagnation plane is of about 270 eV. Let us assume that the composition of c_T/c_D at the separatrix at the stagnation point isidentical to the hydrogen isotope composition in the plasma core: 50 % D and 50 % T.

Based on Tokar's modelling, there is a significant change in the plasma isotope composition in the ITER tokamak reactor scrape-off layer (SOL) along the magnetic field due to the action of thermal forces. With the stoichiometric composition of $c_T = c_D$ at the separatrix in the stagnation plane, the plasma and gas in the divertor contain no more than 10 % tritium. Conversely, reducing c_T along the magnetic field toward the divertors lowers the high-density limit (HDL). Let us assume that the H-L transition occurs at the last closed flux surface, where the temperature varies between 270 eV and 150 eV. In this temperature range, c_T varies between 0.5 and 0.4, according to the Tokar's equations.

The reference pulse with pure deuterium plasma on JET-ILW shows f_{GW}, which agrees well with Goldston's prediction, up to a factor of 0.86: $f_{GW} \approx 0.86 \times f_{GW,Goldston}$. We assume that this factor is machine-independent and apply it for the ITER prediction of HDL.

Goldston's predicted f_{GW} scaling gives an estimated value of $f_{GW} \approx 0.96$ for a 50 %/50 % D-T mixture, considering the main ITER parameters mentioned above. Taking into account the variation of c_T between 0.4 and 0.5 in the region where the H-L transition occurs, f_{GW} ranges from 0.94 to 0.96. The lower boundary is only 10 % higher than the $f_{GW} = 0.85$ projected for ITER in the baseline scenario.

It is important to note that ITER will operate with impurity seeding, which can also influence the HDL. This scaling should be confirmed in dedicated experiments with impurity seeding. Further investigations into the physics of the HDL are required.

5. Conclusion

To comprehend the fundamental mechanisms governing the H-mode density limit in fusion devices with all-metal walls, extensive investigations have been carried out on JET-ILW.

In this study, the influence of the hydrogen isotope mixture on the HDL in the fully metallic machine JET-ILW is investigated for the first time. The H-mode DL experiments with mixed hydrogen isotopes were performed with a divertor warm cryo-pumps where the cryo-panels were cooled with liquid nitrogen (LN_2). By using a reduced divertor pumping speed in the JET-ILW vessel with a warm cryo-pump, we create conditions that closely resemble the base gas pressure on ITER, making our experiments directly relevant. It was shown that the HDL limit is identical for the cold and warm cryo-pump experiments, confirming our earlier statement that detachment does not play a significant role for the H-L transition in fully metallic wall machines [28,7]. In addition, all phases typically observed in cold cryo-pump HDL pulses appear in warm cryo-pump pulses. At the same time, the total gas consumption is reduced by a factor of 13 in the plasma with a warm cryo-pump.

By comparing similar discharges but fuelled with either deuterium or protium, it was found that the HDL limit exhibits a dependence on the isotope mass: the density limit is up to 35 % lower in protium compared to similar deuterium plasma conditions. In mixed HDL plasmas, the maximum achievable density and HDL limit decrease with increasing protium concentration, c_H. The corresponding maximum Greenwald fraction f_{GW} of approximately 1.02 was attained in the pulse with the smallest c_H at 4.4 %. The fraction f_{GW} decreases to 0.96 at $c_H = 48$ %. At the same time, the average atomic mass, $\overline{A}$, of the plasma species decreases in these pulses from 1.96 at $c_H = 4.4$ % to 1.52 at $c_H = 48$ %. Notably, the maximum achievable density remains nearly independent of the applied heating power in both deuterium and protium plasmas, as well as mixed H/D fuelling conditions.

In addition, the measured Greenwald fractions were also compared to a heuristic model based on the SOL pressure threshold for MHD instability, as proposed by Goldston. This comparison specifically examines the theorys reliance on isotopic mass.Notably, the measured Greenwald fractions closely match the predictions from the heuristic model. Slightly higher HDL measured values for c_H concentrations above 30 % can be explained by Tokar's analitical solution, which predicts isotope separation in the SOL and greater c_D concentration at the separatrix in the stagnation point.

The H-mode density limit prediction for the ITER fusion device has been performed based on Tokar's equations and Goldston's scaling. ITER's baseline operation involves a 50 % deuterium–tritium (D-T) mixture, with the separatrix electron temperature around 270 eV. Tokar's analytical solution suggests a change in plasma isotope composition along the magnetic field, impacting the high-density limit (HDL). Using data from JET-ILW and applying a scaling factor, the estimated f_{GW} for ITER is between 0.94 and 0.96 in unseeded scenarios. Impurity seeding and further experiments are needed to refine this prediction.

CRediT authorship contribution statement

A. Huber: Writing – original draft, Validation, Supervision, Resources, Investigation, Formal analysis. **G. Sergienko:** Project administration, Investigation, Formal analysis. **M. Groth:** Project administration, Investigation. **D. Keeling:** Supervision, Project administration, Investigation. **M. Wischmeier:** Validation, Project administration, Formal analysis. **D. Douai:** Project administration. **E. Lerche:** Validation, Investigation, Formal analysis. **C. Perez von Thun:** Formal analysis. **S. Brezinsek:** Supervision, Project administration. **V. Huber:** Writing – original draft, Validation, Supervision, Resources, Investigation, Formal analysis. **A. Boboc:** Investigation. **M. Brix:** Formal analysis. **I.S. Carvalho:** Supervision, Investigation. **A.V. Chankin:** Formal analysis. **E. Delabie:** Formal analysis. **I. Jepu:** Validation. **V. Kachkanov:** Validation. **V. Kiptily:** Formal analysis. **K. Kirov:** Supervision. **Ch. Linsmeier:** Supervision. **E. Litherland-Smith:** Formal analysis. **C.G. Lowry:** Supervision. **C.F. Maggi:** Project administration. **J. Mailloux:** Supervision, Project administration. **A.G. Meigs:** Formal analysis. **Ph. Mertens:** Formal analysis. **M. Poradzinski:** Validation, Formal analysis. **K.-D. Zastrow:** Supervision, Project administration. **M. Zlobinski:** Formal analysis.

Declaration of competing interest

The authors declare that they have no known competing financial interests or personal relationships that could have appeared to influence the work reported in this paper.

Acknowledgement

This work has been carried out within the framework of the EUROfusion Consortium, funded by the European Union via the Euratom Research and Training Programme (Grant Agreement No 101052200 — EUROfusion). Views and opinions expressed are however those of the author(s) only and do not necessarily reflect those of the European Union or the European Commission. Neither the European Union nor the European Commission can be held responsible for them.

Data availability

Data will be made available on request.

References

[1] Progress in the ITER Physics Basis, Edd., 2007 *Nucl. Fusion* **47** S1 sqq.
[2] H. Zohm, et al., Nucl. Fusion 53 (2013) 073019.
[3] M. Greenwald, et al., Plasma Phys. Control. Fusion 44 (2002) R27.
[4] R.J. Goldston, et al., J. Nucl. Mater. 463 (2015) 397–400.
[5] P. Manz et al Nucl. Fusion 2023 63 076026 (23pp).
[6] A. Huber, et al., Nucl. Mater. Energy 12 (2017) 100–110, https://doi.org/10.1016/j.nme.2017.01.005.
[7] M. Bernert, et al., Plasma Phys. Control. Fusion 57 (2015) 014038 (12pp).
[8] A. Huber *et al., Nucl. Fusion* **57** (2017) 086007 (11pp).
[9] Y.R. Martin, et al., J. Phys.: Conf. Series 123 (2008) 012033.
[10] S. Brezinsek et al 2013 Nucl. Fusion 53 083023 (13pp).
[11] R.J.H. Pearce, Fusion Eng. Des. 82 (2007) 1294–1300.
[12] A. Huber, et al., Fusion Eng. Des. 82 (2007) 1327–1334.
[13] U. Kruezi, *et al* 2020 *JINST* **15** C01032.
[14] S. Vartanian, et al., Fusion Eng. Des. 170 (2021) 112511.
[15] D.L. Hillis, et al., Rev. Sci. Instrum. 70 (1999) 359–362.
[16] V.S. Neverov, et al., Nucl. Fusion 59 (2019) 046011.
[17] A.N. Dmitriev, R.S. Ivanov, G.I. Stotskii, Sov. J. Plasma Phys. 10 (1984) 115.
[18] J.D. Hey, et al., J. Phys. b: at. Mol. Opt. Phys. 32 (1999) 3555–3573.
[19] J.D. Hey, et al., J. Phys. b: at. Mol. Opt. Phys. 37 (2004) 2543–2567.
[20] Ph. Mertens, et al., Plasma Phys. Control. Fusion 43 (2001) A349–A373.
[21] W. Eckstein, Computer Simulation of Ion-Solid Interactions, Springer, 1991.
[22] T. Eich, et al., Nucl. Fusion 58 (2018) 034001.
[23] L.C. Bernard, F.J. Helton, R.W. Moore, T.N. Todd, Nucl. Fusion 23 (1983) 1475.
[24] M.A. Makowski, C.J. Lasnier, A.W. Leonard, et al., Nucl. Mater. Energy 12 (2017) 1010–1014.
[25] G. Sergienko et al to be published.
[26] R. Pasqualotto, et al., Rev. Sci. Instrum. 75 (2004) 3891.
[27] M. Tokar, J. Nucl. Mater. 162–164 (1989) 648–651.
[28] A. Huber, et al., J. Nucl. Mater. 438 (2013) S139–S147, https://doi.org/10.1016/j.jnucmat.2013.01.022.
[29] P.C. Stangeby, The Plasma Boundary of Magnetic Fusion Devices, Institute of Physics Publishing, Bristol, UK, 2000.